Chinese Chemical Letters 31 (2020) 3015–3026

Contents lists available at ScienceDirect

Chinese Chemical Letters

journal homepage: www.elsevier.com/locate/cclet

Review

Functionalization of bismuth sulfide nanomaterials for their application in cancer theranostics

Hui Wang[a], Junlei Yang[a], Penghui Cao[a], Ning Guo[a], Yuhao Li[a], Yuefeng Zhao[a], Shuang Zhou[b], Ruizhuo Ouyang[a,*], Yuqing Miao[a]

[a] Institute of Bismuth Science, University of Shanghai for Science and Technology, Shanghai 200093, China
[b] Cancer Institute, Tongji University School of Medicine, Shanghai 200092, China

ARTICLE INFO

Article history:
Received 28 March 2020
Received in revised form 2 May 2020
Accepted 4 May 2020
Available online 12 May 2020

Keywords:
Bi_2S_3
In vivo imaging
Multifunctional nano-system
Diagnosis
Treatment

ABSTRACT

Multifunctional bismuth sulfide (Bi_2S_3) nanomaterials exhibit significant potential as nanomedicines for the diagnosis and treatment of cancer. These nanomaterials act as excellent photothermal agents and radiation sensitizers for the treatment of tumors, and they can also act as contrast agents for computed tomography (CT) imaging, photoacoustic imaging (PA), and other forms of imaging to provide real-time tumor monitoring and testing guidance. Compared with other nanomaterials, Bi_2S_3 nanomaterials can readily adapt to different applications by virtue of the fact that they can be easily functionalized. However, these nanomaterials have some limitations that cannot be ignored and need to be addressed, such as poor biocompatibility, toxicity, and low chemical stability. It is widely believed that appropriate functionalization of Bi_2S_3 nanomaterials could remedy such defects and significantly improve performance. This review summarizes the ways in which Bi_2S_3 nanomaterials can be functionalized and discusses their applications in cancer theranostics over the last few years, focusing particularly on imaging and therapy. We also discuss issues relating to how Bi_2S_3 nanomaterials can be analyzed, including how we might be able to use these systems to inhibit and treat tumors and how current limitations might be overcome to improve treatment efficacy. Finally, we hope to provide inspiration and guidance as to how we might create a more optimized multifunctional nano-system for the diagnosis and treatment of tumors.

1. Introduction

Cancer is still the most serious disease threatening human life, consuming significant medical resources and increasing the financial burden of the families concerned [1]. Over the past few decades, the world has invested enormous human, material and financial resources to allow the exploration of novel methods to overcome cancer. However, the complexity, diversity, and heterogeneity of cancer still creates an enormous obstacle for the development of new diagnostics and therapies [2]. There are many types of malignant tumors associated with different tissues and organs. Furthermore, discrete disease stages respond differently to various treatments. Consequently, there is an urgent need to develop comprehensive treatment protocols. With the rapid development of nanotechnology, nanomaterials are playing an increasingly important role in the field of biomedicine, providing new ideas and methods for the diagnosis and treatment of cancer [3,4]. At present, there are three main modes of cancer treatment: surgical excision, chemotherapy and radiation therapy (RT). However, off-target toxicity and small therapeutic indices lead to severe side effects in patients undergoing chemotherapy; these factors represent major disadvantages for chemotherapy and create significant limitations for the application of chemotherapy [5]. New emerging therapeutic strategies, such as photothermal therapy (PTT) [6,7], photodynamic therapy (PDT) [8], immunotherapy [9], gene therapy and magnetothermal therapy, have shown high anticancer efficacy and are expected to be used routinely in the future clinical treatment of cancer.

An increasing number of nanomaterials have been developed for medical applications, including Au [10], graphene (GO) [11], Bi [10], Fe_3O_4 [12], $MoSe_2$ [13], Co_9Se_8 [14], Bi_2Se_3 [15], TaS_2 [16], Bi_2S_3 [17], CuS [18] and WS_2 [19]. Of these, the development of Bi_2S_3, and its potential application in medicine has aroused significant interest from researchers. Compared with other nanomaterials, Bi_2S_3 is more advantageous for certain applications due to their ability to be functionalized. Through covalent or

* Corresponding author.
E-mail address: ouyangrz@usst.edu.cn (R. Ouyang).

https://doi.org/10.1016/j.cclet.2020.05.003

noncovalent interactions, it is possible to load Bi_2S_3 nanoparticles (NPs) with a range of functional molecules, including chemotherapeutic drugs, fluorescent probes, and other biomolecules. The doping and adsorption of some metals provide additional characteristics, such as electrochemical properties, magnetic properties, radioactivity, as well as imaging and diagnostic capability [20]. Moreover, Bi_2S_3 has a higher X-ray absorption coefficient and stronger contrast than the iodized small molecule computed tomography (CT) contrast agents that have been widely used for CT imaging [21]. Furthermore, Bi_2S_3 has a band gap width of 1.33 eV at room temperature, thus yielding very strong absorption performance in the near infrared region (NIR). Nanomaterials with strong NIR absorption can be used as excellent photothermal agents for the PTT of tumors [22,23].

In this review, we summarize the research carried out thus far on Bi_2S_3 nanomaterials and their applications for tumor therapy, including molecular imaging, therapeutics, and combined therapy (Fig. 1) [24–31]. First, we discuss the physicochemical properties and functionalization of Bi_2S_3 nanomaterials, including shape control, metal doping and surface modification. Not only can functionalized nanomaterials be used for molecular imaging to improve imaging resolution, sensitivity, and to reduce potential damage to normal tissues and systems, they can also be applied as drug carriers to transport drugs effectively to tumor sites and assist treatment. Then, we introduce the use of Bi_2S_3 nanomaterials for cancer treatment, including CT, fluorescence and photoacoustic (PA) imaging techniques, along with PTT, PDT, RT treatment regimens. We place particular emphasis on multifunctional nanomaterials with a simple structure and good biological safety as these can be integrated with multimodal imaging with therapeutic functionality to promote the development of cancer treatment. Finally, we discuss recent studies relating to tumor treatments that were based on Bi_2S_3 nanomaterials and discuss how these might be combined with PTT, PDT, RT, chemotherapy and other treatment methods for the diagnosis and treatment of cancer. Developing such methodology, we should be able to improve patient outcomes.

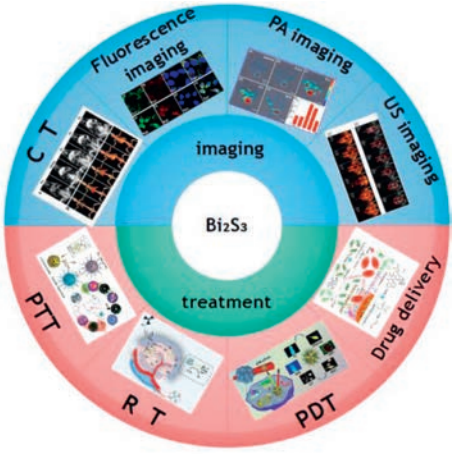

Fig. 1. Applications of Bi_2S_3 nanomaterials in tumor therapy. PTT: Reproduced with permission [24]. Copyright 2018, the Royal Society of Chemistry; RT: Reproduced with permission [25]. Copyright 2019, the Royal Society of Chemistry; PDT: Reproduced with permission [26]. Copyright 2019, Elsevier; Durg delivery: Reproduced with permission [27]. Copyright 2016, the Royal Society of Chemistry; CT: Reproduced with permission [28]. Copyright 2015, the Royal Society of Chemistry. Fluorecence imaging: Reproduced with permission [29]. Copyright 2018, Elsevier; PA imaging: Reproduced with permission [30]. Copyright 2015, American Chemical Society; US imaging: Reproduced with permission [31]. Copyright 2016, the Royal Society of Chemistry.

2. Functionalization of B_2S_3 nanomaterials

As important semiconductor materials with unique properties, Bi_2S_3 nanomaterials have received a significant amount of attention and have been widely used in the field of medicine, thus providing an excellent developmental prospect for the future [32]. However, these nanomaterials have certain limitations which cannot be ignored, such as poor biocompatibility, toxicity, and low chemical stability. The functionalization of Bi_2S_3 nanomaterials could alleviate these defects and thus improve performance. There are three ways in which Bi_2S_3 nanomaterials can be functionalized. (1) Shape control: Bi_2S_3 nanomaterials can be produced in different shapes by controlling the synthesis steps; thus, these materials can be engineered to meet different requirements. However, it is still a significant challenge to develop simple methods to synthesize Bi_2S_3 nanomaterials for medical applications [21]. (2) Metal doping: The properties of Bi_2S_3 nanomaterials can be altered or improved by doping its pure crystal structure [33] (Fig. 2) with another metal element or nanoparticle [20]. (3) Surface modification: Both the structure and state of the surface of Bi_2S_3 nanomaterials can be changed using physical and chemical methods and thus adjust the surface for various applications [34].

2.1. Shape control

The application of nanomaterials mainly depends on their unique physical and chemical properties which are predominantly controlled by the size and morphology of the nanomaterials themselves [35]. For example, Bi_2S_3 nanomaterials have a band gap of only 1.33 eV, thus making these nanomaterials a good prospect for the photothermal treatment of tumors [36] due to their strong NIR absorption performance. However, these nanostructures exhibit irregular morphology and an uneven size distribution. Consequently, Bi_2S_3 nanomaterials are often limited from insufficient light conversion efficiency and low transmission rate. Therefore, controlling the morphology of nanoparticles can enhance their efficacy for specific applications [37]. There are several known morphologies of Bi_2S_3 nanomaterials, including Bi_2S_3 nanodots [38–40]; one-dimensional (1D) Bi_2S_3 nanocrystals, such as nanorods, nanowires and nanotubes [41–45]; and some 2D and 3D nanocrystals, including reticular, disc-like, feather-like, microspheric, sea-urine-like and flower-like structures [46–53]. Bi_2S_3 nanomaterials are mainly synthesized *via* the colloidal solution method [54], photochemical method [55], solvent thermal method [37,56], microwave method [57], hydrothermal

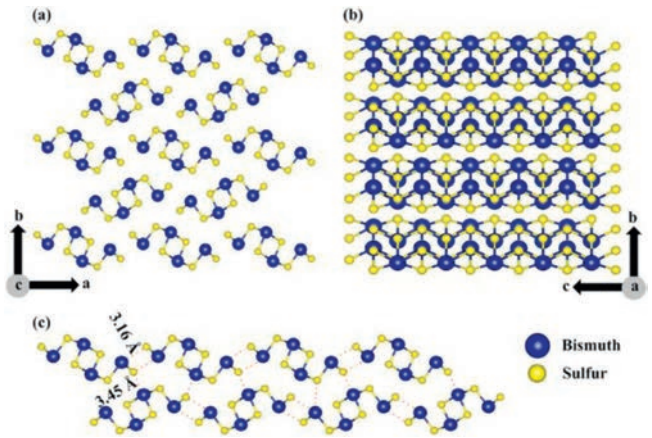

Fig. 2. The crystal structure of Bi_2S_3: (a) a–b and (b) b–c planes, and (c) representation of the crystal showing noncovalent bonding lengths and van der Waals bonds (shown by red dotted lines), along with their lengths. Copied with permission [33]. Copyright 2018, American Chemical Society.

method [58], pyrolysis method [59], reflux method [60], sonochemical method [61], chemical precipitation [35], ion exchange [62], and biological synthesis [63,64]. The morphologies of Bi_2S_3 nanomaterials vary across the different preparation methods. Fig. 3 shows the different morphologies of Bi_2S_3 nanomaterials synthesized by different methods.

The factors that affect the growth dynamics and microstructure development of nanocrystals are crucial for customizing novel nanocrystals and controlling the properties of such materials [50,65]. Therefore, an increasing number of studies have attempted to study the formation and growth of nanocrystals. Shape evolution and phase transition largely depend on specific reaction conditions, including pH value, system temperature and reaction time [35,47,66]. For example, Tang *et al.* described the synthesis of a new Bi_2S_3 nanostructure using a simple colloid solution method incorporating a crystal-splitting growth mechanism. Various forms of Bi_2S_3 can be obtained by controlling the synthesis parameters, including the reaction temperature, the amount of oleic acid, and the addition of precursor. The formation of Bi_2S_3 nanomaterials is often from "simple to complex" and from "low dimension to high dimension" [54].

The Bi_2S_3 nanodots are more suitable for biological and medical fields than large particles because of their slow reorganization and clearance by phagocytes [39,67]. For example, the oleic acid-coated Bi_2S_3 nanodots were prepared in a simple manner by using bismuth neodecanoate as a precursor; this exhibits good biocompatibility, a long circulation time, and does not exert adverse reactions to organs [38]. Recently, green biosynthetic methods have emerged to synthesize Bi_2S_3 nanodots. Bovine serum albumin (BSA) was used to produce Bi_2S_3 nanodots (Bi_2S_3@BSA) in which BSA acted as a stabilizer and provided sulfur to form Bi-S bonds. This is a synthetic method that is not only simple and environmentally friendly but could also synthesize Bi_2S_3@BSA with high chemical stability, no toxicity and good biodegradability [68].

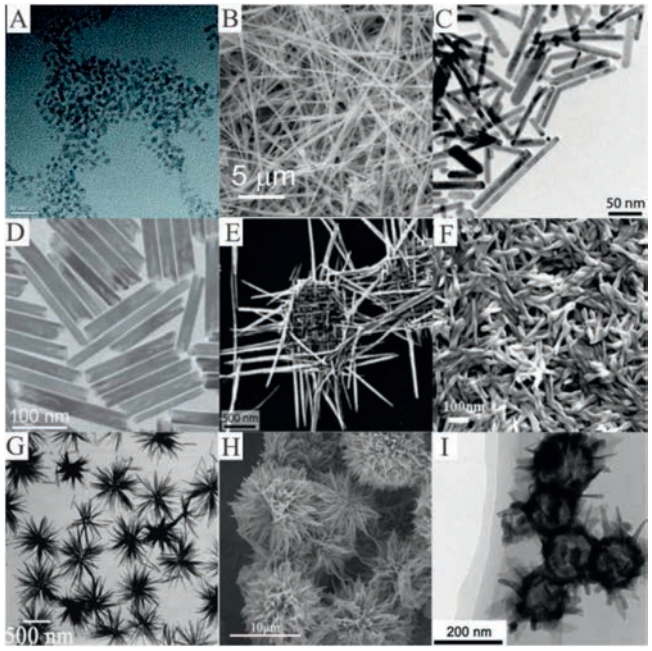

Fig. 3. Images of Bi_2S_3 nanomaterials with different morphologies. (A) Bi_2S_3 nanodots. Reproduced with permission [40]. This figure has been adapted for free from ref [40]. licensed under Creative Commons Attribution-NonCommercial 3.0 Unported (CC BY-NC 3.0) Licence (https://creativecommons.org/licenses/by-nc/3.0/). (B) Bi2S3 nanowires. Reproduced with permission [43]. Copyright 2013, American Chemical Society. (C) Bi_2S_3 nanorods. Reproduced with permission [42]. Copyright 2005, American Chemical Society. (D) Bi_2S_3 nanotubes. Reproduced with permission [41]. This figure has been adapted for free from ref [41]. licensed under the Creative Commons Attribution 4.0 International License of Spring Nature (https://creativecommons.org/licenses/by/4.0/). (E) Disc-like Bi_2S_3 nanorod networks. Reproduced with permission [42]. Copyright 2005, American Chemical Society. (F) Bi_2S_3 nanobundles. Reproduced with permission [45]. Copyright 2016, Elsevier. (G) Bi_2S_3 nanoflowers. Reproduced with permission [48]. Copyright 2011, Elsevier. (H) Bi_2S_3 nanoflowers. Reproduced with permission [47]. Copyright 2009, American Chemical Society. (I) Nanoscale urchins. Reproduced with permission [46]. Copyright 2016, the Royal Society of Chemistry.

The synthesis of 1D Bi_2S_3 nanostructures, such as nanorods, nanowires and nanotubes, have been extensively studied by developing various preparation methods [69,70]; these have sharp surfaces, high aspect ratios [57], fast electron transport capacity, and are expected to exhibit high catalytic activity. As an excellent electronic transport channel, the 1D Bi_2S_3 nanostructures have also been applied in biosensors [71]. Among the 1D nanostructures, Bi_2S_3 nanotubes appear to be the most attractive because they exhibit large numbers of contact areas, including boundaries, internal and external surfaces, and can be easily functionalized within the structural tube. Bi_2S_3 nanotubes are commonly used as nanoscale host materials [72], and show tremendous potential for medicine [73,74].

The 2D Bi_2S_3 nanostructures are predominantly mesh- or disk-shaped and are often used to connect electronic and optoelectronic devices [75]. However, it is quite challenging to synthesize the desired 2D nanostructures through the hierarchical assembly of 1D nanostructures. By using a novel 2D-template-engaged topotactic transformation process, Li *et al.* successfully synthesized a disc-like Bi_2S_3 nanorod network using a BiOCl smooth disk as a template and precursor. The added thioacetamide transformed the BiOCl disk to a disk-shaped Bi_2S_3 nanorod network. Because Bi_2S_3 nanocrystals show a strong tendency to grow into a 1D nanostructure along the c-axis, the resulting Bi_2S_3 bands extend along the c-axis to form a Bi_2S_3 layered structure *via* van der Waals interactions, finally evolving into a disc-like nanorod network [50].

The 3D Bi_2S_3 nanostructures include microspheres, sea urchins and flowers; these structures have been studied extensively. Flower-like Bi_2S_3 nanomaterials possess a larger specific surface area than spherical or rod-like structures, thus leading to a larger receiving area for light; these materials have the potential for broad application in the field of photocatalysis [76,77], and have achieved significant success in hydrogen storage and sensor applications [78,79]. The application of flower-like Bi_2S_3 nanomaterials for the treatment of tumors has yet to be reported, presumably because these structures are too large. In contrast, sea urchin-like Bi_2S_3 nanomaterials, which possess a hollow mesoporous structure, have excellent potential for the treatment of tumors. This is because these nanomaterials have a highly specific surface area and rich mesopores; these can provide a high loading capacity for drugs (or guest biomolecules) used in chemotherapy and for other additional functions [46].

2.2. Metal doping

Metal doping refers to the introduction of other metal elements or nanoparticles into the pure crystal structure. This practice can change the inherent nature of the original atomic layer, such as band gaps and defects, thus increasing conversion efficiency and improving other functions, such as electrochemical and magnetic properties, radiation, imaging, and diagnostic applications. Therefore, the functionalization of Bi_2S_3 nanomaterials plays a vital role in their downstream applications [20].

Doping Bi_2S_3 nanomaterials with different types of metal ions not only enhances the effects of RT and PTT, but also introduces additional functions to achieve multi-mode imaging and collaborative treatments [20]. For example, doping iron, manganese, cobalt, niobium and other magnetic atoms into Bi_2S_3

nanomaterials can improve ferromagnetism for combined imaging and can increase the photothermal treatment effect. In a previous study, Li *et al.* prepared PEGylated Fe@Bi_2S_3 nanocomposite (NCs) for cancer imaging and treatment. The narrow direct band gap provides Bi_2S_3 with strong NIR absorption capacity, thus providing significant potential for the use of Fe@Bi_2S_3 NCs in PTT. The addition of an iron core endows Fe@Bi_2S_3 NCs with magnetic properties and allows these nanoparticles to be used as a magnetic resonance contrast agent, thus providing MRI/CT dual-mode imaging (Fig. 4). These Fe@Bi_2S_3 NCs provide more accurate guidance for the treatment of tumors [24]. Cao *et al.* successfully produced a flower-like Fe_7S_8/Bi_2S_3 superstructure that was assembled by hydrophilic nanomaterials through a simple one-pot solvent heating strategy. At a wavelength of 808 nm, the NIR absorption performance of Fe_7S_8/Bi_2S_3 was significantly improved, and was 1.54 times stronger than pure Bi_2S_3. These nano-low molecules can be used as drug carriers that can control their release under pH/NIR stimulation and show promising chemical-photothermal synergistic therapeutic effects both *in vivo* and *in vitro*. The resulting nano-coagulant depressant opens up a new path for designing other nano-agents with better NIR absorption and chemical/photothermal treatment effects [80]. In a previous study, Li *et al.* developed a core-shell structure by doping Bi_2S_3 NPs with Mn using a cation exchange method; these could be used as a simple and novel platform for diagnosis and treatment at the nanometer level. Mn doping permits MRI and helps to improve the imaging resolution of soft tissue injury. The combination of three-mode imaging guided PTT and RT was successfully achieved for the treatment of cancer, thus overcoming previous limitations associated with excessive treatment exposure and damage to human health [81]. Hexagonal Cu_3BiS_3 nanocrystallines have also been synthesized using a one-pot solvothermal protocol and showed a stronger ability for NIR absorption, a higher CT imaging response, and better hydrophilic properties than single Bi_2S_3 [82].

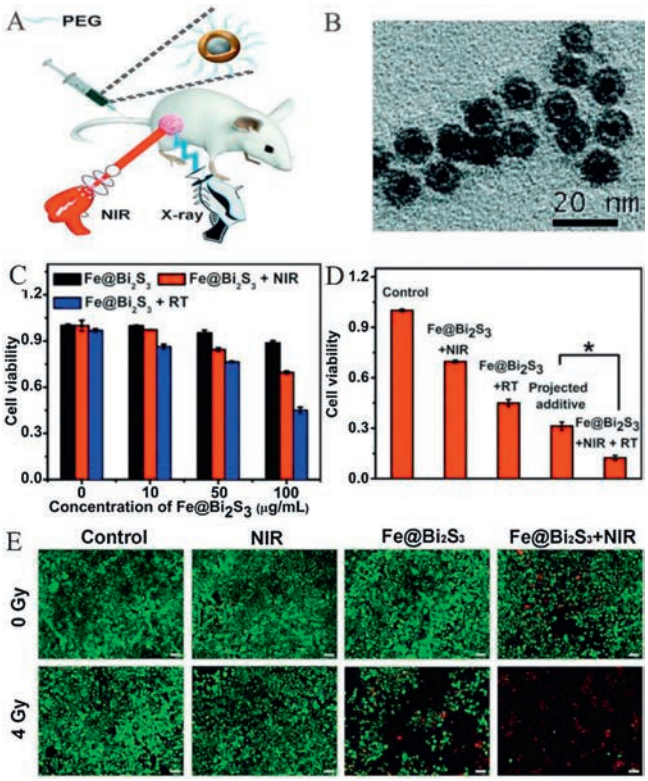

Fig. 4. Bi_2S_3 nanomaterials doped with metal ions. (A and B) An illustration of the combination of PTT with RT and TEM images of PEGylated Fe@Bi_2S_3 NCs, (C and D) quantitative analysis of the cell viability of Fe@Bi_2S_3 NPs with or without NIR-laser irradiation and RT, (E) live-dead staining of 4T1 cells after co-incubation with Fe@Bi_2S_3 NPs and being subjected to RT, NIR and the combined PTT and RT (scale bar: 100 μm). Reproduced with permission [24]. Copyright 2018, the Royal Society of Chemistry.

2.3. Surface modification

The purpose of surface modification is to change the structure and state of the surface of Bi_2S_3 NPs *via* physical and chemical methods in order to control the surface of these NPs. The properties of these nanomaterials can be changed through surface modification, including improved dispersion, increased surface area, and enhanced surface activity; it is also possible to generate new physical, chemical, and mechanical properties on the surface of the nanoparticles [83]. As a result, the efficacy of tumor treatments can be significantly increased due to the improvement in certain properties of the nanomaterials, such as biocompatibility, particle dispersion, cell uptake, targeting ability, specific surface area, biological half-life and toxicity.

Bi_2S_3 NPs can be broadly divided into four categories according to the effects of different modifications, including the addition of polymers to increase biocompatibility [21], biomolecules to enhance specificity [84], metal NPs to improve surface plasma resonance absorption [85], and drugs that can be used for Bi_2S_3-combined therapy.

2.3.1. The modification of Bi_2S_3 NPs with polymers

The surfaces of Bi_2S_3 nanomaterials are often modified with polymers in order to increase biocompatibility and extend the cycle half-life to achieve the best therapeutic effect. Commonly, the polymers used for surface modification include polyvinyl pyrrolidone (PVP), polyethylene glycol (PEG), polyacrylic acid (PAA), polydopamine (PDA) [86,87], chitosan [88,89], polyvinyl alcohol [90], and dendritic macromolecules [21], which usually combine with Bi_2S_3 nanomaterials *via* coordination, electrostatic adsorption, hydrophobic action or other interactions. The amphiphilic ligands, containing both hydrophilic and hydrophobic groups, were used to make the hydrophobic materials water-soluble [91]. The polymer coated on the surface of Bi_2S_3 NPs provides free functional groups on the surface and a foundation for downstream-specific identification and drug-loading functions.

The modification of NPs with PVP has become popular due to three important factors. First, PVP modification can improve biocompatibility and prevent Bi_2S_3 nanomaterials from accumulating over a short time period, thus affecting their biological application. Second, PVP can increase the concentration of bismuth reaching the tumor site and thus enhance contrast for X-ray absorption. Third, the *in vivo* cycle is prolonged; this is because plasma proteins may replace the capping mercaptan and bind to the surface of Bi_2S_3 nanocrystalline; these are rapidly cleared by the reticuloendothelial system. PVP modification can overcome this problem. In a previous study, the water solubility of Bi_2S_3 NPs was greatly improved after being modified by PVP and the PVP-modified Bi_2S_3 NPs had a higher X-ray absorption coefficient, a longer imaging time *in vivo*, and better a better safety profile than iodinated small molecule CT imaging agents [92].

Fang's research group has also developed dendritic polymer stable NCs (Fig. 5A). Dendritic polymer is important because metal ions can first complex with the dendritic polymer through coordination and/or electrostatic interaction, thus allowing the downstream *in situ* conversion of metal ions into corresponding NCs. It has been demonstrated that this material has good biocompatibility, enhanced X-ray attenuation characteristics, and can be further functionalized to serve as an efficient contrast agent for efficient biological system CT imaging [21]. In another study, Li *et al.* modified Bi_2S_3 nanocrystals with amphiphilic 1,2-

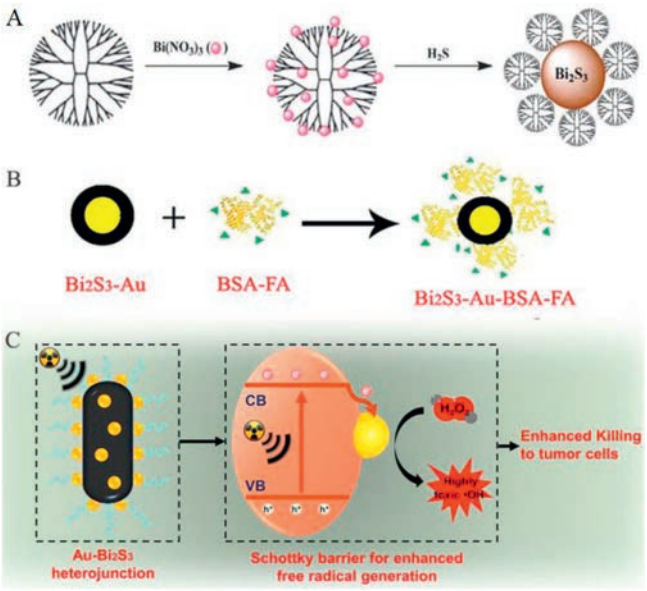

Fig. 5. The surface modification of Bi_2S_3 nanomaterials. (A) Illustration showing the preparation of Bi_2S_3 dendritic polymer stable NCs. Reproduced with permission [21]. Copyright 2013, the Royal Society of Chemistry. (B) Synthetic procedure of Bi_2S_3-Au heterodimer (Bi_2S_3-Au-BSA-FA hybrids) modified with both FA and BSA showing high targeting activity. Reproduced with permission [84]. Copyright 2020, American Chemical Society. (C) Illustration of the therapeutic process based on Au-Bi_2S_3 hetero-nanostructure composites (HNSCs). Reproduced with permission [85]. Copyright 2019, American Chemical Society.

distearoyl-*sn*-glycero-3-phosphoethanol-amine-*N*-[amino(polyethylene glycol)] *via* hydrophobic interactions to prolong the internal circulation time of the synthesized nanomaterials; these particles showed good photothermal properties with no obvious side effects after systemic injection [40]. Lu *et al.* subsequently encapsulated $Cu_{1.94}S$ and Bi_2S_3 nanocrystals into a biocompatible poly (amino acid) matrix of ~85 nm for CT-guided PTT. The lactam ring in the poly-succinimide (PSI) chain was opened as a result of the ammonolysis of OAm to form a PSI_{OAm} with a long hydrophobic side chain [47], and $Cu_{1.94}S$ and Bi_2S_3 were wrapped to form the hydrophilic NCs. The amount and proportion of multiple $Cu_{1.94}S$ and Bi_2S_3 was shown to improve photothermal conversion efficiency (PCE) and CT imaging capability [93].

2.3.2. The modification of Bi_2S_3 NPs with biomolecules

Besides controlling the size and shape of nanomaterials, some biomolecules are used to modify nanomaterials to improve targeting ability so as to allow drugs to reach the target tumor area more quickly. Imaging or treatment relies on the specific aggregation of the material at the tumor site, thus increasing the concentration difference between the lesion and the surrounding normal tissues. A significant body of research has been performed in an attempt to deliver drugs to the tumor site accurately and efficiently. There are two forms of targeting, passive targeting and active targeting. Passive targeting refers to the enhanced permeability and retention (EPR) effect and pH response; active targeting refers to the use of biological molecules, such as peptides, enzymes, and antibodies, to modify the surface of Bi_2S_3 nanomaterials such that the nanomaterials exhibit a higher binding force with the membrane of cancer cells [94,95].

For passive targeting, the size of Bi_2S_3 nanomaterials prepared by a range of methods are usually very small such that Bi_2S_3 nanomaterials can accumulate in large quantities in tumor sites, leading to effective passive targeting. NPs with small particle sizes (<100 nm) are known to yield a better tumor distribution than larger NPs [96]. The basic principle here is that the blood vessels at the tumor site are more permeable than normal vessels due to the twists, leaks, and irregularities of the blood vessels, as well as the absence of blood vessel walls at the tumor site [97]. Larger nanomaterials are easily absorbed by phagocytes and experience difficulty in reaching the diseased tissues through the blood vessels. In contrast, nanomaterials of a smaller size can escape from phagocytes and end up in tumor cells for much longer time periods [98].

Bi_2S_3 is usually modified with biomolecules to achieve active targeting. These biomolecules include peptides [99], antibodies [100], folic acid (FA) [101], HA [102], arginine-glycine-aspartic acid (RGD) [103], and biotin [104]; all of these biomolecules exhibit high binding affinity with the membrane of cancer cells. The modification of biomolecules for active targeting cannot only improve the compatibility of Bi_2S_3 nanomaterials, but can also drive them to target specific cells. For example, Lu *et al.* prepared the mesoporous silica-coated Bi_2S_3 NPs that were modified with RGD peptide using the *N*-hydroxysuccinimide ester of polyethylene glycol maleimide as a covalent linker. These showed high specificity for osteosarcoma. Furthermore, the accumulation rate for this nanomaterial in tumor cells was 10 times higher than that in the surrounding normal tissues, leading to significantly enhanced ablation of osteosarcoma when PTT was combined with chemotherapy [103]. In a previous study, Kinsella *et al.* reported the synthesis of CGNKRTRGC (Lyp-1)-labeled Bi_2S_3 NPs. After being treated with 1,2-diastearoyl-*sn*-glycero-3-phosphoe-thanol-amine-*N*-[methoxy(polyethylene glycol)], Bi_2S_3 NPs were easily modified by Lyp-1 peptides due to the thioether formation between the maleimide and the N-terminal cysteine portion of Lyp-1. Lyp-1 is the first peptide to show specific homing of tumor lymphatic vessels and other cells in tumor tissues. The accumulation of Lyp-1-labeled NPs at the tumor site was significantly greater compared with unlabeled NPs [99]. In another study, FA was successfully used as a targeting molecule to identify tumor cells through modifying the Bi_2S_3-Au-BSA heterodimer. Briefly, after the biomineralization of Bi_2S_3 with BSA, Au NPs grew *in situ* on Bi_2S_3-BSA surface, followed by the FA functionalization using EDC and NHS (Fig. 5B). The prepared Bi_2S_3-Au-BSA-FA hybrids could accumulate effectively at tumor sites due to the good targeting capability and showed enhanced permeability and retention [84]. Trastuzumab (Tam) is a monoclonal antibody targeting the overexpression of HER-2 in breast cancer cells, and can specifically recognize the HER-2 receptor on SKBR-3 breast cancer cells that are HER-2 positive. A new mesoporous silica-coated Bi_2S_3 nanomaterial (Bi_2S_3@mPS) was prepared and successfully attached to Tam *via* the abundant Si-OH groups on the surface. Both *in vitro* and *in vivo* studies demonstrated that Tam-Bi_2S_3@mPS exhibited good biocompatibility and drug-loading capacity, along with accurate and active tumor targeting and accumulation [100].

2.3.3. The modification of Bi_2S_3 NPs with metal NPs

Precious metals, such as gold, silver, platinum, palladium, and their oxides, are often used to functionalize Bi_2S_3 NPs in order to strengthen their treatment efficacy. The purpose of metal modification is to increase surface plasmon resonance and the PCE to implement a combined form of tumor treatment [20]. For example, Wang *et al.* developed Au functionalized Bi_2S_3 nanomaterials with a Schottky heterostructure (Au-Bi_2S_3) (Fig. 5C) based on the strong interaction between Au and Bi_2S_3, not simply a physical mix. Owing to the Schottky potential barrier between Au and the semiconductor Bi_2S_3, the electrons generated by X-ray can be captured and transferred to Au, thus separating the electron hole pairs. As a result, the rate of utilization for X-ray induced low energy electrons is significantly improved in the course of RT, and free radicals can be produced even in low oxygen environments, thus enhancing the effect of cancer RT [85]. In a previous paper, Li

et al. produced MnO_2 NPs coated with BSA-Bi_2S_3 NCs through biomineralization for cancer therapy. The presence of MnO_2 obviously increased the absorbance of BSA-Bi_2S_3-MnO_2 NPs (100 mmol/L) at a wavelength of 808 nm in a solution of 100 mol/L H_2O_2, generating a large amount of O_2 within 30 s; this helped to improve tumor hypoxia and enhanced tumor treatment [25]. Guo *et al.* further developed a novel Gd-doped Bi_2S_3 NCs (Bi_2S_3-Gd) which showed good stability and biocompatibility for the CT/MRI-guided PTT of cancer *in vitro*; these NPs improved contrast and enhanced imaging for CT and MRI when low concentrations of Bi and Gd were involved, thus improving the accuracy of diagnosis [36].

2.3.4. The loading of Bi_2S_3 NPs with drugs

The combination of Bi_2S_3 with chemotherapy drugs is also receiving significant attention for researchers involved in developing new forms of cancer treatment. Certain drugs can help Bi_2S_3 to kill tumors faster and more effectively. In turn, Bi_2S_3 can act as a carrier to deliver drugs to the target tumor area so as to achieve more effective treatment. Cancer cells can be killed quickly upon the absorption of chemotherapy drugs [105], such as doxil (DOX) [106], paclitaxel (PTX) [107], docetaxel (Dtxl) [108], cisplatin [109,110], quercetin and gemcitabine [109]. Within the molecular structures of anticancer drugs, there are usually a range of functional groups, including hydroxyl groups, carboxyl groups, amino groups, and benzene ring structures. These functional groups can directly or indirectly interact with the materials used for treatment through charge attraction, coordination, intermolecular forces, and chemical bonds, thus forming nanocomposites. Following the induction of certain conditions (involving light, heat, acid, redox and enzymes), the drug molecules in the complex system can be released slowly and thus exert their anticancer effects.

Hollow mesoporous silica is believed to represent an ideal form of drug nano-carrier and has a large and specific surface area. As a drug carrier, drug molecules can be loaded within the channel structure of mesoporous silica through hydrogen bonding and electrostatic forces. Meanwhile, the good biocompatibility and non-toxicity of hollow mesoporous silica ensures the safety of SiO_2 as a drug-carrier that can release their cargo in an efficient manner [26,103,111]. For example, Ma *et al.* prepared a novel form of Bi_2S_3 NPs by surfactant induced condensation, which were coated with mesoporous silica (BMSN). Results showed that BMSNs exhibited high DOX loading efficiency (45 wt%) along with pH-responsive drug release control; these characteristics arose due to electrostatic interaction between the silane surface and the DOX molecules (Fig. 6). Compared with free DOX, embedding DOX in BMSNs could significantly improve the therapeutic effect of these NPs toward multidrug resistant cancer cells [112].

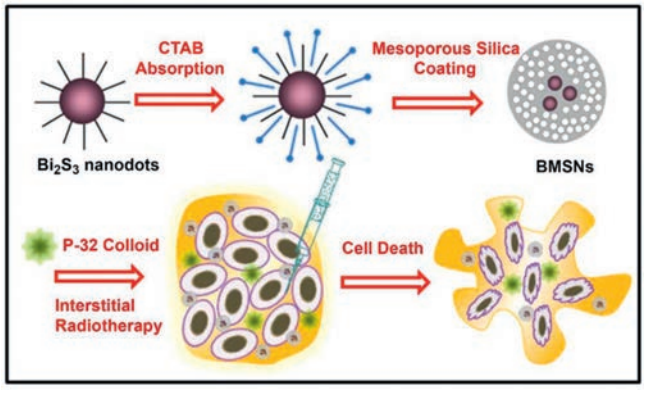

Fig. 6. Schematic demonstration of the synthesis of Bi_2S_3 NPs coated with mesoporous silica (BMSNs) for the application in interstitial therapy. Copied with permission [112]. Copyright 2015, Elsevier.

In addition to using mesoporous structures to load drugs, another option is to encapsulate them. For example, Zhao *et al.* synthesized an alginate (AG)-based phase change injection hydrogel consisting of AG/MoS_2/Bi_2S_3-poly(ethylene glycol)/DOX (MBP) for image-guided tumor heat treatment and chemotherapy. The release of encapsulated drug molecules can be controlled under acidic conditions. Following NIR laser irradiation, such systems would not only show good photothermal treatment effects, but also the heat converted by the MBP promoted the diffusion of the drug from the hydrogel, thus releasing the drug on demand and improving the efficiency of chemotherapy [113].

Bi_2S_3 nanomaterials can be designed to combine drugs with different capabilities for different cancer treatments. Drugs can help Bi_2S_3 to kill tumors faster and more effectively. For example, Song *et al.* used Bi_2S_3 as a carrier and successfully loaded the PI3K inhibitor through electrostatic adsorption, LY294002. Under the stimulation of an 808 nm laser, the release rate of LY294002 at the tumor site was accelerated. The release of LY294002 inhibited the activity of PI3K and protein kinase B and subsequently activated the expression of glycogen synthase kinase 3 which not only accelerated the apoptosis of tumor cells, but also significantly inhibited the expression of HSP70, thus improving the hyperthermia sensitivity of tumor cells under mild conditions [59].

3. The application of Bi_2S_3 in oncological medicine

Increasing amounts of research attention are now been paid to the application of Bi_2S_3 nanomaterials for the diagnosis and treatment of cancer, a major threat to human health [114]. Here, we systematically summarize the latest progress of how Bi_2S_3 nanomaterials are being applied in biomedicine, particularly in the diagnosis and treatment of cancer (Table 1). There are several noninvasive diagnostic imaging methods available to us, including ultrasound (US), CT, MRI, single photon emission computed tomography (SPECT), positron emission tomography (PET), fluorescence imaging [115], and PA imaging. Each method has its own advantages and limitations [116]. There are also several major cancer treatments, including chemotherapy, RT, PTT, PDT, hyperthermia, and magnetic therapy [27,30,31,117–121]. Over recent years, PTT has attracted considerable interest from researchers due to its noninvasive application, minimal side effects, and high selectivity [122].

3.1. Tumor characteristics

Tumors arise because of the abnormal differentiation of normal cells. In order to inhibit and eliminate tumors effectively, targeted measures need to be designed in order to eliminate a particular tumor according to its growth characteristics and environmental conditions. Tumors have three major characteristics that need to be considered. First, at the tumor site, blood vessels zig-zag and tend to leak. Vessels also tend to be irregular and the tumor vessel wall is missing, thus resulting in greater permeability in the tumor part of the blood vessels than in normal blood vessels. Secondly, spontaneous capillaries are relatively fragile with poor heat dissipation ability; this is due to the special blood circulation of tumor cells. Clinical experiments have proved that, in general, cancer cells can be killed at 42 °C in 2 h, while normal tissue cells can tolerate 42–43 °C for a longer time period; the safety tolerance limit for normal cells is 45 °C. Currently, it is generally accepted that the effective temperature for tumor hyperthermia is 45 °C. Thirdly, tumor sites do not usually have a sufficient oxygen supply and therefore present with unique hypoxic and acidic conditions.

Table 1
The application of Bi_2S_3 nanomaterials in the diagnosis and treatment of tumors.

Material	Tumor cell	NIR Absorption (laser)	Application	Ref.
Tween-Bi_2S_3	4T1	808 nm (1 W/cm^2) for 10 min	PTT+CT/MSOT	[30]
PVP-rGO/Bi_2S_3@DOX	BEL-7402	808 nm (1 W/cm^2) for 10 min	PTT/chemotherapy+CT/PAT	[27]
BNN-Bi_2S_3	BEL-7402	808 nm (1 W/cm^2) for 10 min	PTT	[117]
Bi_2S_3-PEG@DOX	HeLa	808 nm (1 W/cm^2) for 5 min	PTT/chemotherapy+CT/PA	[46]
Au-Bi_2S_3	HeLa	808 nm (0.3 W/cm^2) for 10 min	PTT/RT+IR	[85]
Bi_2S_3	4T1	808 nm (0.75 W/cm^2) for 15 min	RT/PTT+CT/PA	[118]
Bi_2S_3-PLGA	PC3		RT+PA	[119]
BSA-Bi_2S_3-MnO_2	U14	808 nm (0.4 W/cm^2) for 20 min	RT/PTT+CT	[25]
BSA-Gd_2O_3/Bi_2S_3	4T1	785 nm (1.5 W/cm^2) for 5 min	PTT+CT/PA/MRI	[120]
CS/MBP-DOX	HT29	808 nm (1 W/cm^2) for 5 min	PTT	[121]
Cu_3BiS_3	TC71	915 nm (1.2 W/cm^2) for 10 min	PTT/RT/IR	[82]
Fe@Bi_2S_3-PEG	4T1	808 nm (1 W/cm^2) for 5 min	PTT/RT+CT/MRI	[24]
FLBS-PFH-NPs	L02		HIFU+US/CT	[31]
MnS@Bi_2S_3-PEG	4T1	808 nm (0.8 W/cm^2) for 5 min	PTT/RT+CT/MRI/PA	[81]
PEG-Bi_2S_3	4T1	808 nm(3 W/cm^2) for 5 min	PTT+CT	[40]
DOX-Bi_2S_3@BCA	L929 and HepG2	808 nm (1.5 W/cm^2) for 5 min	PTT/chemotherapy	[17]
RGD-Bi_2S_3@MSN	UMR-106	808 nm (1 W/cm^2) for 10 min	PTT/chemotherapy+CT	[103]
Bi_2S_3@LY294002	LoVo	808 nm (0.6 W/cm^2) for 10 min	PTT	[59]

rGo: graphene; BNN: bis-*N*-nitroso compounds; PLGA: poly(lactic-*co*-glycolic acid); CS: chitosan; FLBS-PFH-NPs: folate targeted perfluorohexane NPs carrying Bi_2S_3; BCA: alginate; RGD: arginine-glycine-aspartic acid; MSN: mesoporous silica.

The traditional methods for treating cancer involve surgical excision and radiation therapy. However, these methods can exert significant side effects. In recent years, new therapeutic methods have emerged that aim to reduce such side effects, including PTT, PDT, and immunotherapy. These methods take advantage of the fact that tumor cells cannot tolerate heat or low pH.

3.2. The application of Bi_2S_3 nanomaterials in image diagnosis

Imaging diagnosis is a critical aspect of the cancer treatment process, providing real-time guidance for diagnosing disease, guiding treatment, and monitoring treatment responses [30]. Bi_2S_3 nanomaterials have been used successfully for CT imaging and other imaging modalities, such as fluorescence, PA, and US.

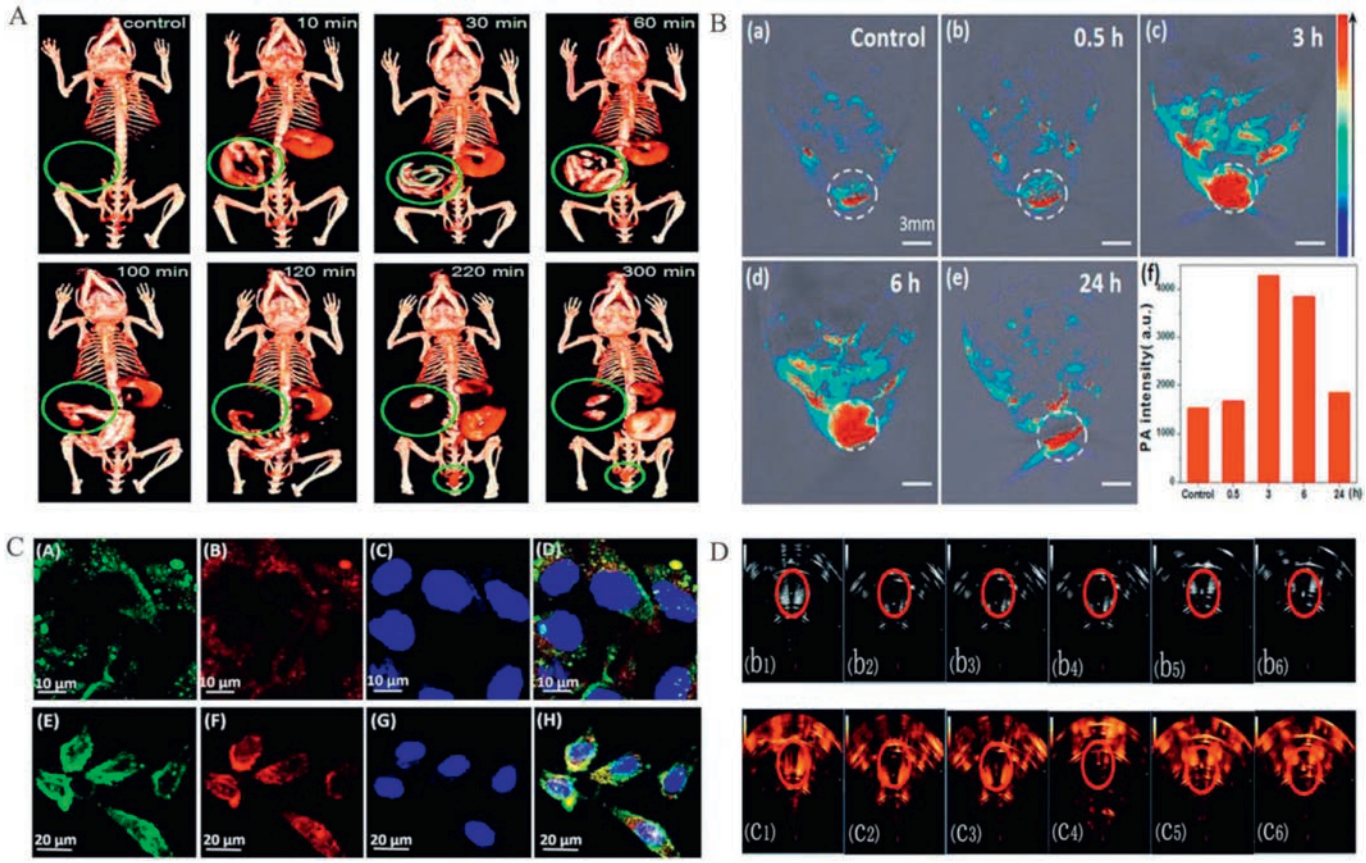

Fig. 7. (A) CT imaging of the GI tract in BALB/c nude mice at different intervals after the oral administration of Bi_2S_3@SiO_2 NRs. Reproduced with permission [28]. Copyright 2015, the Royal Society of Chemistry. Serial CT coronal views following intravenous injection of PVP-coated Bi_2S_3 nanodots solution, and the corresponding 3D renderings of a rat. (B) Confocal laser scanning microscope (CLSM) images of HepG2 cells after incubation with polyethylene glycol chitosan NPs (BSA-Bi_2S_3-CG-PEG NPs) for 30 min. Reproduced with permission [29]. Copyright 2018, Elsevier. (C) MOST images of a tumor and the intensity of photoacoustic signals in the tumor before and after the intravenous injection with Bi_2S_3 NRs at different time points (0.5, 3, 6 and 24 h). Reproduced with permission [30]. Copyright 2015, American Chemical Society. (D) US images of Bi_2S_3 NPs in B mode and contrast mode before and after phase transformation at different HIFU acoustic power levels. Reproduced with permission [31]. Copyright 2016, the Royal Society of Chemistry.

3.2.1. The use of Bi_2S_3 in CT imaging

CT is a noninvasive imaging examination technology. Bi_2S_3 nanomaterials have been used as CT contrast agents for some time now, largely owing to their high capacity and long circulation times in organisms, long residence time, low toxicity, fast clearance and cost-effectiveness. Compared with traditional iodate contrast agents, Bi_2S_3 nanomaterials have more advantages and can improve the sensitivity and accuracy of detection [92,123]. For example, Ai *et al.* prepared Bi_2S_3 NPs with a particle size of only 2–3 nm with good monodispersity; these showed lower levels of cytotoxicity, better biocompatibility, more constant *in vivo* circulation time, and higher CT imaging contrast than iodine [38]. In another study, Fang *et al.* successfully synthesized Bi_2S_3 using dendrimer as a stabilizer, showing higher X-ray attenuation intensity than iodine-based small molecule CT contrast agents. Clear CT images were obtained from the subcutaneous injection area of rabbits, and blood pool CT imaging of mice was possible by intravenous injection. thus indicating the significant potential of Bi_2S_3 nanomaterials for CT imaging [21]. In another study, Zheng *et al.* prepared Bi_2S_3@SiO_2 nanorods (NRs) for the noninvasive real-time imaging of the gastrointestinal tract (GI) (Fig.7A). The fusion of PAT and CT provided critical supplementary information by yielding anatomical details with high spatial resolution [28].

3.2.2. The use of Bi_2S_3 in fluorescence imaging

Fluorescence is a common luminescence phenomenon, and most NIR materials have fluorescence properties to some extent. Fluorescence imaging is advantageous because it is associated with high sensitivity, low costs, and simple operation. Wang *et al.* previously prepared polyethylene glycol chitosan NPs (BSA-Bi_2S_3-CG-PEG) with embedded Bi_2S_3; these exhibited dual-wavelength fluorescence and were thus used for the fluorescence imaging and PTT of HepG2 cells [29]. When excited at 488 nm and 633 nm, the prepared materials emitted strong luminescence near 570 nm and 660 nm, respectively, without the addition of any other luminescent materials. Both of these fluorescence emission bands are far away from spontaneous biological light. The fluorescence imaging capability of this material can be attributed to the cross-linking reaction of chitosan and glutaraldehyde in an acidic environment (Fig. 7B).

3.2.3. The use of Bi_2S_3 in PA imaging

PA imaging is actually an extension of the photothermal effect. When a light-absorbing tissue or material is irradiated by a pulsed laser, local heating and cooling will occur, causing local pressure changes that can be detected ultrasonically and reconstructed into images. By combining multispectral photoacoustic tomography (MSOT)/CT imaging with Bi_2S_3 NRs in PTT, Liu *et al.* were able to overcome defects associated with poor contrast, limited penetration depth, and low resolution during soft tissue CT imaging. Following NIR irradiation, the photoacoustic effect produced by thermal expansion enables soft tissues to obtain higher spatial resolution, which improves the feasibility and accuracy of diagnosis (Fig. 7C). Finally, it has been demonstrated that Bi_2S_3 NRs cannot only be used as a powerful CT contrast agent for angiography and organic imaging, but can act as a contrast enhancer for the real-time MSOT monitoring of tumors in the presence of NR at tumor sites [30].

3.2.4. The use of Bi_2S_3 in US imaging

US imaging is a common clinical diagnostic method with the advantages of real-time monitoring, high levels of safety and sensitivity, low cost, availability, and portability. Huang *et al.* successfully constructed a multifunctional nano-treatment platform based on Bi_2S_3 nanomaterials that were embedded with a polylactic acid-glycolic acid compound capsule (Bi_2S_3-PLGA) and demonstrated that high efficiency radiotherapy sensitization under US guidance [119]. The Bi_2S_3 PLGA capsule showed good contrast-enhanced imaging performance in nude mice with prostate tumors, and could accurately indicate the location of radioactive sources. In another study, Zhou *et al.* prepared a nanoscale phase conversion lipid from FA-targeted perfluorohexane and Bi_2S_3, in which the perfluorohexane was converted from liquid to gas by heating and ultrasonic spokes in order to enhance the cavitation effect of HIFU therapy. The encapsulated Bi_2S_3 NPs gave the material enhanced CT imaging and US imaging capabilities (Fig. 7D). In addition, guided by FA, the prepared nanomaterials could penetrate the leaking blood vessels of tumors and effectively accumulated within the tumors. As a result, significant advancement was achieved in US and CT dual-mode imaging technology and the synergistic therapeutic efficiency of HIFU ablation [31].

3.3. The application of Bi_2S_3 NPs in tumor therapy

Over recent years, there has been unprecedented development in the use of Bi_2S_3 nanomaterials in the field of therapeutic diagnostics. Owing to their unique optical properties and electronic drug-loading properties, Bi_2S_3 nanomaterials play a significant role in therapeutic diagnostics. Indeed, Bi_2S_3 nanomaterials have been widely used in PTT, RT, PDT, immunotherapy, and a range of other fields; they have also been used as a nanocarrier for adjuvant chemotherapy.

3.3.1. PTT

PTT refers to a therapy that uses a NIR irradiation photothermal conversion reagent with good permeability properties for biological tissues in order to generate high levels of heat in localized locations and inducing cancer cell death and tumor necrosis [124]. This localized form of therapy is simple, effective, and causes mild pain with quick recovery; this is referred to as “green therapy” because it causes few side effects in normal human tissues [116]. Compared with traditional methods for the treatment of tumors (such as RT and chemotherapy), PTT is noninvasive, safe, and effective, and has received considerable attention in both clinical application and scientific research. In general, photothermal treatment uses NIR light ranging from 700 nm to 1100 nm. Due to the relatively low absorption and scattering of hemoglobin and water molecules within the transmission window of human tissues, NIR can penetrate into deep tissues by up to 10 cm, thus overcoming the shortcomings of visible light that cannot penetrate tissues well [125]. Tumor cells have a specific form of blood circulation; the capillaries within tumors are relatively fragile and heat dissipation capacity is poor. Bi_2S_3 nanomaterials have been shown to accumulate effectively at tumor sites and generate high levels of heat to kill tumor cells when exposed to NIR irradiation. In a previous study, Zhang *et al.* were able to treat tumors effectively by using the photothermal characteristics of Bi_2S_3 NPs; Bi_2S_3 NPs were combined with bis-*N*-nitroso compounds (BNN) in order to release NO during photothermal treatment to enhance the sensitivity of tumor cells and the overall effect of photothermal treatment. Furthermore, Xiao *et al.* synthesized PVP-modified Bi_2S_3 NRs with a PCE as high as 64.3%. Under NIR laser irradiation, the photothermal performance of these PVP-modified Bi_2S_3 NRs was excellent at the tumor site, thus leading to the effective photothermal ablation of cancer cells *in vivo* and *in vitro* (Figs. 8A and B) [126].

3.3.2. RT

RT is one of the most promising cancer treatments and has been used globally to treat various cancers for many years. This form of therapy ionizes water molecules in organisms *via* high-energy X or Y-ray radiation at the tumor site, thus producing a large amount of

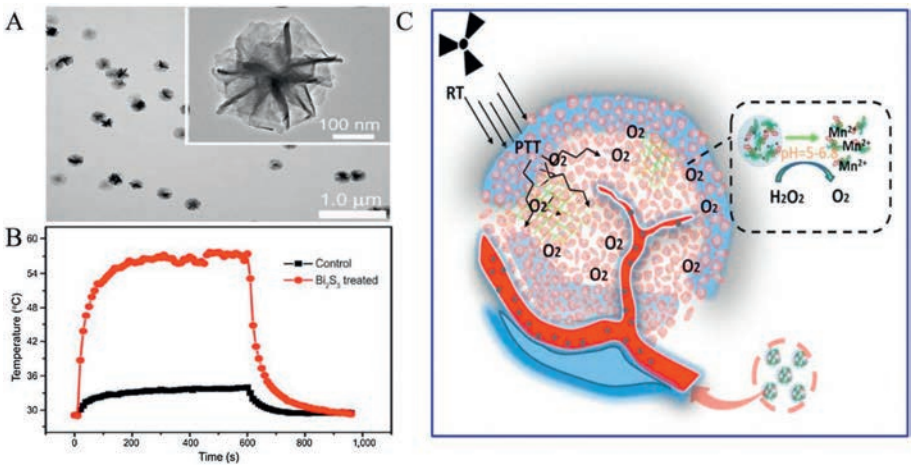

Fig. 8. (A) TEM images of Bi_2S_3 nanoflowers; (B) Temperature curves of the responding mice *versus* time in the control and Bi_2S_3 treated groups under laser irradiation. Reproduced with permission [126]. Copyright 2016, Spring Nature. (C) Schematic illustration for the synthesis of BSA-Bi_2S_3-MnO_2 NCs by biomineralization for enhanced RT. Reproduced with permission [25]. Copyright 2019, the Royal Society of Chemistry.

active oxygen free radicals to kill cancer cells [127]. Due to the X-ray sensitization capability of Bi-based NPs, Bi_2S_3 represents a popular enhancement agent for RT [68]. However, due to the fact that hypoxic tumors are not sensitive to ionizing radiation, and because the normal tissues around the tumor are inevitably damaged, there are still obstacles in providing the optimal conditions for RT. In order to solve these defects, various nanomaterials have been developed to exhibit free radical enhancement and thus act as radiation sensitizers to improve the efficacy of RT. For example, Zhang *et al.* designed BSA-Bi_2S_3-MnO_2 NCs using a biomineralization method. The photothermal effect induced by these BSA-Bi_2S_3-MnO_2 NCs further alleviated tumor microenvironment abnormalities (TME), including hypoxia, acidosis, and extracellular matrix density, and thus improved the RT effect and the treatment efficiency for cervical cancer (Fig. 8C) [25]. Using the GEANT4-based simulation method, Alejo-Martinez *et al.* determined the kinetic energy spectrum of secondary electrons generated by X-ray interaction with Au, Bi_2S_3, and Ta_2O_5 NPs. These authors then calculated the interaction process, energy deposition, absorption dose, and effective distance distribution, of secondary electrons generated by the interaction of 100 million incident photons in the prepared NPs. These experiments showed that Bi_2S_3 and Ta_2O_5 NPs were viable alternatives to Au NPs as dose enhancers for RT [128].

3.3.3. PDT

PDT refers to the generation of oxygen free radicals by photosensitizers in biological tissues after exposure to light. The cytotoxicity of reactive oxygen species (ROS), such as singlet oxygen, can induce apoptosis and necrosis in target organs, and has been widely used for the clinical treatment of tumors [129,130]. Generally, three aspects need to be considered for PDT: excitation light source, photosensitizer and free oxygen. It is very important to select the appropriate photosensitizer in order to produce the best PDT results. Nanomaterials are generally applied for PDT in two ways: One is to use the material itself as a photosensitizer; the other is that the photosensitizer acts as a carrier [131]. However, it is difficult to generate these specific photodynamic properties in Bi_2S_3 nanomaterials due to rapid electron-hole recombination within a narrow band. However, Cheng *et al.* were able to generate a Bi_2S_3-polymer-zinc protoporphyrin IX nanosystem using a thermosensitive polymer that links zinc protoporphyrin IX (ZP) with Bi_2S_3 NRs. In this case, the polymer retracted after being affected by light and heat, thus bringing ZP closer to the Bi_2S_3 NRs. This separates the electrons and holes, thus generating ROS and providing the Bi_2S_3 NRs with a powerful photodynamic capability [132]. PDT requires an aerobic environment, while the rapid growth of the tumors and immature tumor blood vessels often lead to internal hypoxia. High concentrations of the reducing agent L-glutathione (GSH) in cells can also seriously reduce the oxidative damage effect induced by PDT. The combination of PDT and PTT can also improve the curative effect because the high temperatures increase the rate of blood flow and oxygen supply at the tumor site [133].

3.3.4. Chemotherapy

As carriers, Bi_2S_3 nanomaterials help drugs to reach a tumor site efficiently; drugs then assist Bi_2S_3 in killing tumors faster and more effectively. Sun *et al.* loaded Bi_2S_3 NCs with the chemotherapy drug DOX and the chloride ion e6 photosensitizer (Ce6) to prepare a multifunctional (BPDC) NCs to improve heat sensitivity at the tumor site. Under laser irradiation, these modified particles produced good PCE and achieved the on-demand release of DOX but did not produce ROS. Developing the perfect combination of PTT, PDT, and chemotherapy, could inhibit tumor growth in a very effective manner [26].

3.4. Multi-mode imaging and collaborative therapy

Two or more biomedical imaging methods are usually used in combination after treatment as this practice can yield more reliable diagnostic results than a single method. A significant body of research has been carried with regards to combining multi-modal imaging technology with treatment technology. The construction of multifunctional nanomaterials is a key requisite in our quest for multimode collaborative therapy, a technique that has already been widely accepted [124]. Bi_2S_3 nanomaterials have significant photothermal effect and are often combined with RT, PDT, immunotherapy, and chemotherapy, to achieve synergistic therapy.

3.4.1. PTT+RT therapy guided by dual-mode imaging (CT+PA)

Although many remarkable achievements have been made in the research and development of RT sensitizers, hypoxia often occurs at tumor sites, thus leading to insensitivity to RT and reduced toxicity to cancer cells. Moderate levels of hyperthermia have been found to increase blood flow at tumor sites and improve the hypoxic environment during heat treatment, thus leading to an

increase in cell radio sensitivity. In addition, the limitations created by the contrast differences in soft tissue during CT imaging, and the limitations imposed by optical imaging depth and resolution, can actually complement each other. Therefore, PTT is often combined with RT and uses CT to assist PA in order to achieve better therapeutic effects.

For example, Bi_2S_3 NRs have been prepared previously and used as a contrast agent for CT and PA imaging; ion these experiments, Bi_2S_3 NRs enhanced the lethal effect of RT by increasing the local radiation dose, and enhanced the anti-tumor effect of RT by increasing the photothermal effect, thus providing a simple and efficient nano-platform for the treatment of tumors (Figs. 9A–G) [118]. This work overcomes the limitations of contrast differences associated with CT imaging in soft tissue and by optical imaging depth and resolution. Wang *et al.* prepared MoS_2/Bi_2S_3-PEG nanosheets by using a solvent thermal method to assist with tumor diagnosis guided by CT/PA imaging with integrated PTT and RT. Following modification, Bi_2S_3 NPs exhibited good X-ray attenuation performance and radiation sensitization effects, thus providing good capability for photothermal and radiation treatment [134].

3.4.2. Dual-mode imaging (CT+PA) guided PTT+chemotherapy

Chemotherapy uses chemical drugs to kill cancer cells. Chemotherapy drugs, such as DOX, can inhibit DNA replication and prevent the rapid proliferation and division of cancer cells. However, chemotherapy drugs are not selective and can also kill normal cells. Consequently, chemotherapy is associated with significant side effects. Bi_2S_3 nanomaterials are often used as nanocarriers to deliver drugs to tumor sites and control drug release on demand. Small molecule drugs such as DOX, PTX, or other chemicals, are widely used in clinical and laboratory settings, and can be easily packaged with Bi_2S_3. In a previous study, Zheng *et al.* prepared a thermo-sensitive hydrogel composed of MoS_2/Bi_2S_3-PEG (MBP) which showed good biocompatibility for the *in vivo* hyperthermia and chemotherapy of colon cancer. Using this system, DOX and MBP nanosheets were encapsulated in a gel system that prevented the DOX-loaded hydrogel from entering the blood stream and damaging normal tissues and cells. Furthermore, the heat generated during photothermal conversion could regulate the rate of drug release rate to ensure continuous on-demand chemotherapy [121].

Another new system that is still being explored is PVP-functionalized rGO/Bi_2S_3 (PVP-rGO/Bi_2S_3) for the synergistic treatment of cancer by chemotherapy and PTT; this system has shown significant inhibitory effects on cancer cells. The combination of the dual mode imaging guidance provided by photoacoustic tomography (PAT) and CT enabled more accurate real-time monitoring (Fig. 9H). Because of the excellent photothermal conversion properties of Bi_2S_3, and the controllable release of DOX triggered under NIR laser, the therapeutic effects of PVP-rGO/Bi_2S_3 NRs were good and involved a combination of hyperthermia and

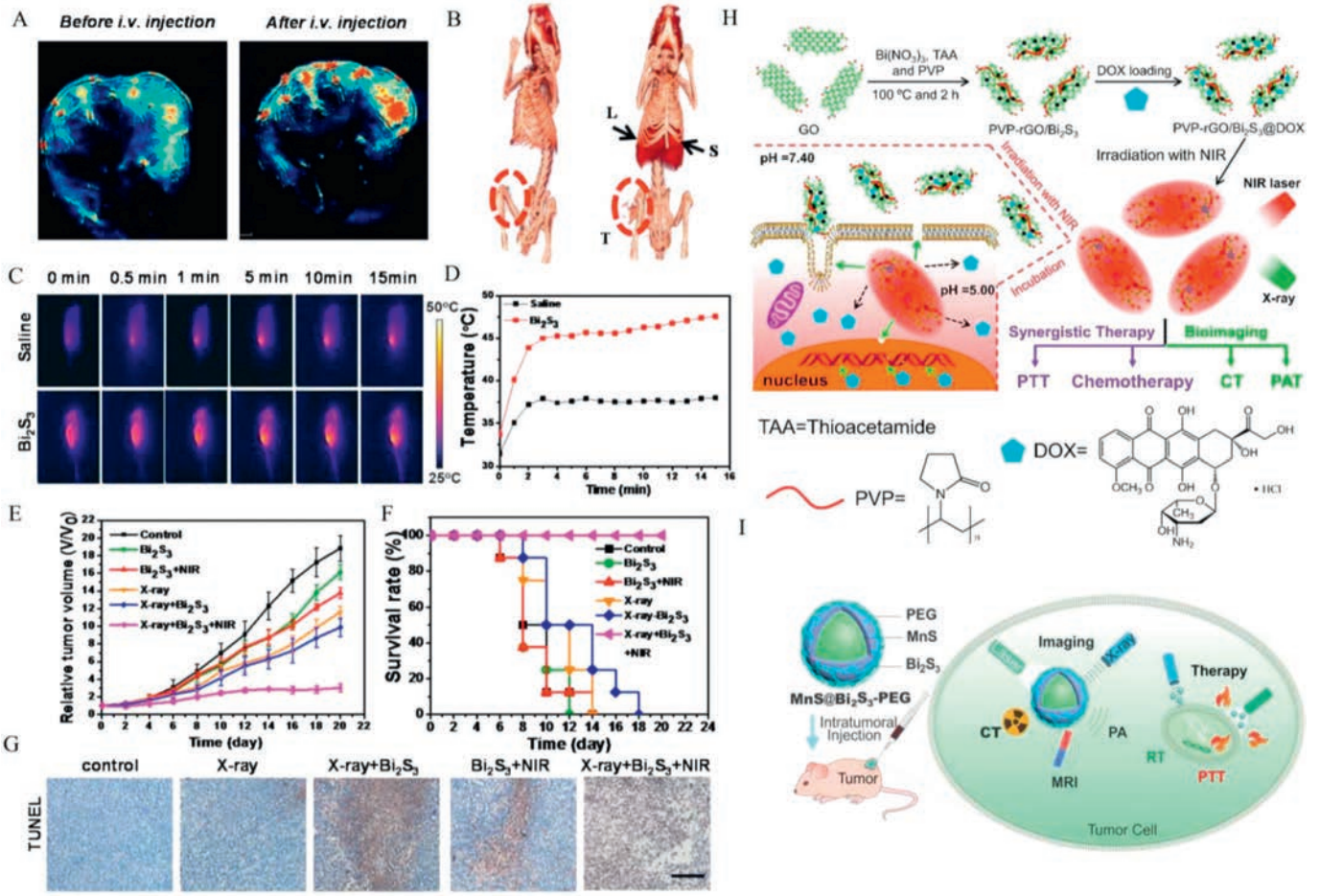

Fig. 9. (A–G) Dual-modal imaging and enhanced radiation therapy combined with photothermal treatment *in vivo*. Reproduced with permission [118]. This figure has been adapted for free from Ref. [118] licensed under the Creative Commons Attribution 4.0 International License of Spring Nature (https://creativecommons.org/licenses/by/4.0/). (H) The synthesis of PVP-rGO/Bi_2S_3 NRs and combination of chemo-photothermal therapy. Reproduced with permission [27]. Copyright 2016, the Royal Society of Chemistry. (I) Synthesis of MnS@Bi_2S_3 nanostructure for the application in highly efficient cancer theranostics. Reproduced with permission [81]. Copyright 2017, the Royal Society of Chemistry.

chemotherapy [27]. In another study, Wu *et al.* designed an injectable multifunctional hydrogel that could undergo a phase change by cooling a hot AG solution containing photoadsorption MBP NPs and drugs. In this previous research, the AG gel formed *in situ* and was then used as a macroscopic blood vessel to retain MBP and DOX, thus providing a critical option for PTT and chemotherapy guided by CT/PA dual-mode imaging [135].

3.4.3. PTT guided by multimodal imaging (MR/PA/CT)

Different imaging techniques, with their own unique properties, are often used together to provide more accurate and reliable tumor identification or real-time therapeutic monitoring. This may require extensive exploration of nanomaterials with multiple imaging properties. For example, Lv *et al.* reported the synthesis of new Gd_2O_3/Bi_2S_3 hybrid nanopoints; these were approximately 4.5 nm in size and showed good monodispersity. These Gd_2O_3/Bi_2S_3 nanopoints could be used as high performance nanometer thermal sensitizers and could be combined with multi-mode enhanced imaging to carry out the photothermal ablation of tumors. Gd_2O_3/Bi_2S_3 nanopoints were helpful for MR imaging with good spatial resolution, PA imaging with microscopic spatial resolution, as well as CT imaging with macroscopic anatomical localization. Under the guidance of multi-mode imaging, PTT achieved satisfactory therapeutic effects, and significantly reduced the possibility of tumor recurrence and metastasis. In addition, the Gd/Bi mole ratio can be independently adjusted to optimize the imaging effect [120]. In addition, a core-shell $MnS@Bi_2S_3$ nanostructure was successfully applied to a tri-modal imaging guided thermo-radio therapy, including MRI, CT, and PA imagings, which could fully capture tumor details because of the strong near-infrared absorption and X-ray attenuation abilities without causing any obvious toxicity *in vivo*, showing excellent therapeutic effect at low dose [81] (Fig. 9I).

4. Conclusions and perspectives

In summary, Bi_2S_3 nanomaterials provide excellent candidates for potential application in the field of medicine. Here, we systematically reviewed the recent advances in research relating to Bi_2S_3 nanomaterials and their applications in the field of tumor therapy, including molecular imaging, therapeutics and combined therapy. Due to their higher X-ray absorption coefficient and stronger contrast than small iodine CT contrast agents, Bi_2S_3 nanomaterials have been widely applied in CT imaging. Furthermore, strong NIR absorption ensures that Bi_2S_3 nanomaterials act as excellent photothermal agents for PTT because almost no NIR absorption occurs within biological tissues. In addition, it is easy to functionalize the surface of Bi_2S_3 nanomaterials with a variety of functional molecules, including chemotherapeutic drugs, fluorescent probes, and biological macromolecules. This allows us to make improvements to imaging resolution or sensitivity, enhancing material targeting, as well as reducing potential impact on normal tissues. More importantly, researchers have emphasized the development of multi-functional Bi_2S_3 nanomaterials with simple structures, good biological safety, and the ability to facilitate multi-modal imaging and cancer therapy.

Although the positive role of Bi_2S_3 nanomaterials in the diagnosis and treatment of tumors has been proven by many studies, continuous efforts are still required to enhance the efficacy of Bi_2S_3 nanomaterials for specific applications. The efficient release of high dose chemotherapy drugs to kill cancer cells in a specific manner remains a key goal but is difficult to realize. Consequently, there is a real need to design Bi_2S_3 nanomaterials with special surface properties, high drug loading rates and fast release rates. Moreover, the toxicity of nanomaterials cannot be ignored when applied in biomedical scenarios. Thus, further research is needed to verify how these nanomaterials are cleared by specific organisms. Finally, PTT can release autoantigens from tumors while immunotherapy can reduce the probability of tumor recurrence and metastasis. Considering their excellent capability for PTT, Bi_2S_3 nanomaterials are expected to be applied in the field of immunotherapy to remove metastasized cancer cells by activating the body's immune system.

Declaration of competing interest

The authors declare no conflicts of interest in this manuscript.

Acknowledgment

This work was financially supported by the Shanghai Natural Science Foundation (Nos. 19ZR1434800, 19ZR1461900).

References

[1] C.E. DeSantis, C.C. Lin, A.B. Mariotto, et al., CA Cancer J. Clin. 64 (2014) 252–271.
[2] W.P. Fan, B. Yung, P. Huang, X.Y. Chen, Chem. Rev. 117 (2017) 13566–13638.
[3] D. Yang, F. Deng, D. Liu, et al., Asian J. Pharm. Sci. 14 (2019) 349–364.
[4] P.N. Navya, A. Kaphle, S.P. Srinivas, et al., Nano Converg. 6 (2019) 23.
[5] S. Yaghoubi, M.H. Karimi, M. Lotfinia, et al., J. Cell. Physiol. 235 (2020) 31–64.
[6] J. Yu, C. Yang, J. Li, et al., Adv. Mater. 26 (2014) 4114–4120.
[7] D. Jaque, L. Martinez Maestro, B. del Rosal, et al., Nanoscale 6 (2014) 9494–9530.
[8] J. Schwiertz, A. Wiehe, S. Grafe, B. Gitter, M. Epple, Biomaterials 30 (2009) 3324–3331.
[9] S.L. Topalian, C.G. Drake, D.M. Pardoll, Cancer Cell 27 (2015) 450–461.
[10] Z. Zhang, J. Wang, C. Chen, Theranostics 3 (2013) 223–238.
[11] M. Xu, J. Zhu, F. Wang, et al., ACS Nano 10 (2016) 3267–3281.
[12] Z. Gao, X. Liu, Y. Wang, et al., Dalton Trans. 45 (2016) 19519–19528.
[13] Y. Wang, F. Zhang, Q. Wang, et al., Nanoscale 10 (2018) 14534–14545.
[14] X.R. Song, X. Wang, S.X. Yu, et al., Adv. Mater. 27 (2015) 3285–3291.
[15] A. Gupta, R.K. Chowdhury, S.K. Ray, S.K. Srivastava, Nanotechnology 30 (2019) 435204.
[16] Y. Liu, X. Ji, J. Liu, et al., Adv. Funct. Mater. 27 (2017) 1703261.
[17] Q. Zou, F. Hou, H. Wang, et al., Eur. Polym. J. 115 (2019) 282–289.
[18] J. Sheng, L. Wang, Y. Han, et al., Small 14 (2018) 1702529.
[19] L. Cheng, J. Liu, X. Gu, et al., Adv. Mater. 26 (2014) 1886–1893.
[20] C. Murugan, V. Sharma, R.K. Murugan, G. Malaimegu, A. Sundaramurthy, J. Control. Release 299 (2019) 1–20.
[21] Y. Fang, C. Peng, R. Guo, Analyst 138 (2013) 3172–3180.
[22] B. Hildebrandt, P. Wust, O. Ahlers, Crit. Rev. Oncol. Hemat. 43 (2002) 33–56.
[23] L. Ren, X. Liu, T. Ji, et al., ACS Appl. Mater. Inter. 11 (2019) 45467–45478.
[24] E.D. Li, X.J. Cheng, Y.Y. Deng, Biomater. Sci.-UK 6 (2018) 1892–1898.
[25] L. Zhang, Q. Chen, X. Zou, et al., J. Mater. Chem. B: Mater. Biol. Med. 7 (2019) 5170–5181.
[26] L. Sun, M. Hou, L. Zhang, et al., Nanomedicine 17 (2019) 1–12.
[27] R. Dou, Z. Du, T. Bao, et al., Nanoscale 8 (2016) 11531–11542.
[28] X. Zheng, J. Shi, Y. Bu, et al., Nanoscale 7 (2015) 12581–12591.
[29] K. Wang, J. Zhuang, Y. Liu, et al., Carbohydr. Polym. 184 (2018) 445–452.
[30] J. Liu, X. Zheng, Z. Gu, C. Chen, Y. Zhao, Nanomed. Nanotechnol. Biol. Med. 12 (2016) 486–487.
[31] D. Zhou, C. Li, M. Hea, M. Mac, J. Mater, Chem. B 4 (2016) 4164–4181.
[32] Y. Yan, K. Chang, T. Ni, K. Li, Mater. Lett. 245 (2019) 158–161.
[33] N. Dhar, N. Syed, M. Mohiuddin, et al., ACS Appl. Mater. Inter. 10 (2018) 42603–42611.
[34] M. Khafaji, M. Zamani, M. Golizadeh, O. Bavi, Biophys. Rev. 11 (2019) 335–352.
[35] Y. Ramos Reynoso, A. Martinez-Ayala, M. Pal, F. Paraguay-Delgado, N.R. Mathews, Adv. Powder Technol. 29 (2018) 3561–3568.
[36] H. Guo, X. Zhao, H. Sun, H. Zhu, H. Sun, Nanotechnology 30 (2019) 075101.
[37] A. Sarkar, A.B. Ghosh, N. Saha, et al., J. Colloid Interface Sci. 483 (2016) 49–59.
[38] K. Ai, Y. Liu, J. Liu, Adv. Mater. 23 (2011) 4886–4891.
[39] A.A. Mansur, F.P. Ramanery, L.C. Oliveira, H.S. Mansur, Carbohydr. Polym. 146 (2016) 455–466.
[40] Z. Li, K. Ai, Z. Yang, et al., RSC Adv. 7 (2017) 29672–29678.
[41] D. Wang, C. Hao, W. Zheng, et al., Nano Res. 2 (2010) 130–134.
[42] M.B. Sigman, B.A. Korgel, Chem. Mater. 17 (2005) 1655–1660.
[43] Q. Yang, C. Hu, S. Wang, Y. Xi, K. Zhang, J. Phys. Chem. C 117 (2013) 5515–5520.
[44] Z.H. Ge, P. Qin, D. He, et al., ACS Appl. Mater. Inter. 9 (2017) 4828–4834.
[45] H. Chen, T. Huang, S. Zheng, T. Fang, L. Wang, Mater. Lett. 185 (2016) 67–71.
[46] Z. Li, Y. Hu, M. Chang, et al., Nanoscale 8 (2016) 16005–16016.
[47] H. Zhou, S. Xiong, L. Wei, et al., Cryst. Growth Des. 9 (2009) 3862–3867.
[48] Z. Chen, M. Cao, Mater. Res. Bull. 46 (2011) 555–562.
[49] W. Liu, C.F. Guo, M. Yao, et al., Nano Energy 4 (2014) 113–122.
[50] L. Li, N. Sun, Y. Huang, Adv. Funct. Mater. 18 (2008) 1194–1201.
[51] A. Phuruangrat, T. Thongtem, S. Thongtem, Mater. Lett. 63 (2009) 1496–1498.

[52] S. Vadivel, V.P. Kamalakannan, N. Keerthi, Balasubramanian, Ceram. Int. 40 (2014) 14051–14060.
[53] J. Chen, S. Qin, G. Song, et al., Dalton Trans. 42 (2013) 15133–15138.
[54] J. Tang, A.P. Alivisatos, Nano Lett. 6 (2006) 2701–2706.
[55] J. Zhang, W. Zhang, Z. Yang, Appl. Surf. Sci. 257 (2011) 6239–6242.
[56] Y. Xu, Z. Ren, G. Cao, et al., Physica B: Condens. Matter 405 (2010) 1353–1358.
[57] B. Zeng, W. Liu, W. Zeng, C. Jin, J. Nanosci, Nanotechno. 19 (2019) 2276–2280.
[58] M. Salavati-Niasari, D. Ghanbari, F. Davar, J. Alloys. Compd. 488 (2009) 442–447.
[59] L. Song, X. Dong, S. Zhu, et al., Adv. Healthc. Mater. 7 (2018) 1800830.
[60] R. Chen, M.H. So, C.M. Che, H. Sun, J. Mater, Chem. 15 (2005) 4540–4545.
[61] J. Geng, L. Jiang, J. Zhu, Sci. China Chem. 55 (2012) 2292–2310.
[62] J. Wang, L. Li, H. Yu, F. Guan, D. Wang, Inorg. Chem. 58 (2019) 12998–13006.
[63] S. Naveenraj, R.V. Mangalaraja, J.J. Wu, A.M. Asiri, S. Anandan, RSC Adv. 6 (2016) 16215–16222.
[64] I. Uddin, A. Ahmad, E.A. Siddiqui, S.H. Rahaman, S. Gambhir, Curr. Top. Med. Chem. 16 (2016) 2019–2025.
[65] V.N. Richards, S.P. Shields, W.E. Buhro, Chem. Mater. 23 (2011) 137–144.
[66] C. Tojo, M. Dios, F. Barroso, Materials 4 (2011) 55–72.
[67] M. Aresti, M. Saba, R. Piras, et al., Adv. Funct. Mater. 24 (2014) 3341–3350.
[68] H. Nosrati, J. Charmi, M. Salehiabar, F. Abhari, H. Danafar, ACS Biomaterials Sci. Eng. 5 (2019) 4416–4424.
[69] Z. Liu, S. Peng, Q. Xie, et al., Adv. Mater. 15 (2003) 936–940.
[70] D. Chai, X. Yuan, B. Yang, Y. Qian, Solid State Commun. 148 (2008) 444–447.
[71] F. Gao, J. Song, B. Zhang, et al., Chin. Chem. Lett. 31 (2020) 181–184.
[72] X.P. Shen, G. Yin, W.L. Zhang, Solid State Commun. 140 (2006) 116–119.
[73] N. Badea, M.M. Craciun, A.S. Dragomir, et al., Mater. Chem. Phys. 241 (2020) 122435.
[74] M. Safavipour, M. Kharaziha, E. Amjadi, F. Karimzadeh, A. Allafchian, Talanta 208 (2020) 120369.
[75] X. Liu, S. Zhang, S. Guo, et al., Chem. Soc. Rev. 49 (2020) 263–285.
[76] G.Q. Zhao, Y.J. Zheng, Z.G. He, T. Nonferr, et al., Metal. Soc. 28 (2018) 2002–2010.
[77] F.J. Chen, Y.L. Cao, D.Z. Jia, J. Colloid Interfa. Sci. 404 (2013) 110–116.
[78] M. Zhang, D.J. Chen, R.Z. Wang, et al., Mat. Sci. Eng. C: Mater. 33 (2013) 3980–3985.
[79] B. Zhang, X.C. Ye, W.Y. Hou, Y. Zhao, Y. Xie, J. Phys. Chem. B 110 (2006) 8978–8985.
[80] Q. Cao, X. Guo, W. Zhang, et al., Dalton Trans. 48 (2019) 3360–3368.
[81] Y. Li, Y. Sun, T. Cao, et al., Nanoscale 9 (2017) 14364–14375.
[82] B. Li, K. Ye, Y. Zhang, et al., Adv. Mater. 27 (2015) 1339–1345.
[83] X. Ma, Y. Zhao, X.-J. Liang, Acc. Chem. Res. 44 (2011) 1114–1122.
[84] F. Abhari, J. Charmi, H. Rezaeejam, et al., ACS Sustain. Chem. Eng. 8 (2020) 5260–5269.
[85] X. Wang, C. Zhang, J. Du, et al., ACS Nano 13 (2019) 5947–5958.
[86] Z. Li, Y. Hu, K.A. Howard, et al., ACS Nano 10 (2016) 984–997.
[87] R. Chen, C. Zhu, Y. Fan, et al., ACS Appl. Bio. Mater. 2 (2019) 874–883.
[88] S. Banihashem, M.N. Nezhati, H.A. Panahi, Carbohydr. Polym. 227 (2020) 115333.
[89] L. Guo, H. Chen, N. He, Y. Deng, Chin. Chem. Lett. 29 (2018) 1829–1833.
[90] N. Davis, D. Liu, A.K. Jain, et al., Photochem. Photobiol. 57 (1993) 641–647.
[91] Z. Chen, C. Wu, Z. Zhang, et al., Chin. Chem. Lett. 29 (2018) 1601–1608.
[92] O. Rabin, J.M. Perez, J. Grimm, G. Wojtkiewicz, R. Weissleder, Nat. Mater. 5 (2006) 118–122.
[93] X. Lu, Y. Li, X. Bai, Sci. China Mater. 60 (2017) 777–788.
[94] J.A. Barreto, W. O'Malley, M. Kubeil, et al., Adv. Mater. 23 (2011) H18–H40.
[95] T. Sun, Y.S. Zhang, B. Pang, et al., Angew. Chem. Int. Ed. 53 (2014) 12320–12364.
[96] C. Ju, R. Mo, J. Xue, et al., Angew. Chem. Int. Ed. 53 (2014) 6253–6258.
[97] H. Hashizume, P. Baluk, S. Morikawa, et al., Am. J. Pathol. 156 (2000) 1363–1380.
[98] X. Yang, G. Liu, Y. Shi, et al., Nanotechnology 29 (2018) 222001.
[99] J.M. Kinsella, R.E. Jimenez, P.P. Karmali, et al., Angew. Chem. Int. Ed. 50 (2011) 12308–12311.
[100] L. Li, Y. Lu, C. Jiang, et al., Adv. Funct. Mater. 28 (2018) 1704623.
[101] L. Dong, P. Zhang, X. Liu, et al., ACS Appl. Mater. Inter. 11 (2019) 7774–7781.
[102] S. Kim, M.J. Moon, S. Poilil Surendran, Y.Y. Jeong, Pharmaceutics 11 (2019) 306.
[103] Y. Lu, L. Li, Z. Lin, et al., Adv. Healthc. Mater. 7 (2018) 1800602.
[104] M. Bagheri, S. Shateri, H. Niknejad, A.A. Entezami, J. Polym. Res. 21 (2014) 567.
[105] K.D. Mjos, C. Orvig, Chem. Rev. 114 (2014) 4540–4563.
[106] M. Li, W. Song, Z. Tang, et al., ACS Appl. Mater. Inter. 5 (2013) 1781–1792.
[107] P. Ma, R.J. Mumper, J. Nanomed, Nanotechol. 4 (2013) 1000164.
[108] D.J. Stewart, Crit. Rev. Oncol. Hematol. 63 (2007) 12–31.
[109] C. Serri, V. Quagliariello, R.V. Iaffaioli, et al., J. Cell. Physiol. 234 (2019) 4959–4969.
[110] R.A. Alderden, M.D. Hall, T.W. Hambley, J. Chem. Educ. 83 (2006) 728–734.
[111] Y. Gao, Y. Chen, X. Ji, et al., ACS Nano 5 (2011) 9788–9798.
[112] M. Ma, Y. Huang, H. Chen, et al., Biomaterials 37 (2015) 447–455.
[113] J. Zhao, J. Li, C. Zhu, et al., ACS Appl. Mater. Inter. 10 (2018) 3392–3404.
[114] E.M. Ward, C.E. DeSantis, C.C. Lin, et al., CA Cancer J. Clin. 65 (2015) 481–495.
[115] K. Wang, J. Zhuang, L. Chen, et al., Colloids Surf. B: Biointerfaces 160 (2017) 297–304.
[116] P. Xue, R. Yang, L. Sun, et al., Nano-Micro Lett. 10 (2018) 74.
[117] X. Zhang, J. Du, Z. Guo, et al., Adv. Sci. 6 (2019) 1801122.
[118] X. Cheng, Y. Yong, Y. Dai, et al., Theranostics 7 (2017) 4087–4098.
[119] Y. Huang, M. Ma, S. Chen, et al., RSC Adv. 4 (2014) 26861–26865.
[120] X. Lv, X. Wang, T. Li, et al., Small 14 (2018) 1802904.
[121] Y. Zheng, W. Wang, J. Zhao, et al., Carbohydr. Polym. 222 (2019) 115039.
[122] Y. Cheng, Y. Feng, H. Jian, Z. Tang, H. Zhang, Angew. Chem. Int. Ed. 57 (2017) 246–251.
[123] Y. Liu, K. Ai, L. Lu, Acc. Chem. Res. 45 (2012) 1817–1827.
[124] V. Shanmugam, S. Selvakumar, C.S. Yeh, Chem. Soc. Rev. 43 (2014) 6254–6287.
[125] K. Dong, Z. Liu, Z. Li, J. Ren, X. Qu, Adv. Mater. 25 (2013) 4452–4458.
[126] Z.Y. Xiao, C.T. Xu, X.H. Jiang, et al., Nano Res. 9 (2016) 1934–1947.
[127] M. Babaei, M. Ganjalikhani, Bioimpacts 4 (2014) 15–20.
[128] H. Alejo-Martinez, A.C. Sevilla-Moreno, A. Ondo-Mendéz, J.H. Quintero, C.J. Páez, J. Phys.: Conf. Ser. 1247 (2019) 012050.
[129] A.T. Lau, Y. Wang, J.F. Chiu, J. Cell. Biochem. 104 (2008) 657–667.
[130] Y.Y. Wang, Y.C. Liu, H.W. Sun, D.S. Guo, Coord. Chem. Rev. 395 (2019) 46–62.
[131] J.T. Xu, W. Han, P.P. Yang, et al., Adv. Funct. Mater. 28 (2018) 1803804.
[132] Y. Cheng, Y. Chang, Y. Feng, et al., Adv. Mater. 31 (2019) 1806808.
[133] Z. Yang, Z. Sun, Y. Ren, et al., Mol. Med. Report. 20 (2019) 5–15.
[134] S. Wang, X. Li, Y. Chen, et al., Adv. Mater. 27 (2015) 2775–2782.
[135] C. Wu, J. Zhao, F. Hu, et al., Carbohydr. Polym. 180 (2018) 112–121.